A sugar transporter as a candidate for the outer hair cell motor

Gwénaëlle S.G. Géléoc[1], Stefano O. Casalotti[2], Andrew Forge[2] and Jonathan F. Ashmore[1]

[1]Department of Physiology, University College London, Gower Street, London WC1 E6BT, UK

[2]Institute of Laryngology and Otology, University College London, 330-332 Gray's Inn Road, London WC1 X8EE, UK

Correspondence should be addressed to J.A. (j.ashmore@ucl.ac.uk)

Forces developed by cochlear outer hair cells (OHCs) are responsible for the sharp tuning that underlies sensitivity and frequency selectivity in the ear. OHCs exhibit a voltage-dependent motility involving a 'motor' protein embedded in the basolateral membrane. The motor has so far resisted molecular identification. Here we provide evidence that it may be related to a fructose transporter. We show that OHCs are able to transport this sugar selectively and that the sugar alters electrical properties of the OHC motor. These data can be combined into an integrated model of a sugar carrier, that makes the novel prediction, demonstrated here, that such 'neutral' transporters can be voltage dependent.

In mammals, an underlying mechanical amplification expands the sensitivity of the auditory system and enhances the frequency selectivity of the cochlea. The mechanism, known as the 'cochlear amplifier'[1], involves a population of cells, the outer hair cells (OHCs) of the organ of Corti, which act as both sensors and force generators[2,3]. OHCs rapidly change length on membrane polarization[4], using a mechanism that is independent of ATP hydrolysis[5,6] and calcium[7] and that does not depend on microtubule or actin systems[6,8]. The motor candidate is a voltage-sensitive molecule (or assembly of molecules) able to change area when the membrane potential changes, and can be observed as a high-density particle array in the basolateral membrane of the cell[8]. Associated with the OHC electromotility is a charge movement detectable in whole-cell[9,10] and in membrane patch recordings[11] that is thought to arise from a dipole reorientation accompanying the conformational change of the molecule.

Several candidates for the OHC motor molecule have been proposed. One possibility is that it is a modified anion exchanger linked to the underlying cytoskeleton[12,13]. A difficulty with this suggestion is that removal of extracellular anions[14] or disruption of the cytoskeleton[15] has little effect on voltage-dependent charge movement in OHCs. Another possibility is that the motor is a modified ion channel that retains its voltage sensor but has lost ionic permeability. The rate of OHC charge movement (relaxation time constant less than 10 μs[14,16]) is, however, faster than reported for ion channel sensors. A third possibility is that the motor molecule is an electroneutral transmembrane transporter.

Among the membrane proteins present in OHCs, the sugar transporter GLUT5 can be identified immunohistochemically in the basolateral membrane of gerbil OHCs[17]. This transporter is a member of the facilitative glucose transporter family (GLUT) and is specific for fructose. We show here that guinea-pig OHCs transport fructose but also that this sugar interacts with the electrical properties of the OHC motor. We demonstrate that the presence of sugars, and fructose in particular, alters the voltage sensitivity of the charge movement. The simplest explanation is that the charge movement is a hitherto unidentified property of the sugar transporter and reflects the kinetics of conformational change in the carrier. As predicted by this model, our data show that sugar transport is altered by voltage in OHCs. These results support the hypothesis that the OHC motor is closely related to this transporter molecule.

Results

Physiological evidence for sugar transport in OHCs

To maintain osmotic balance when a solute is transported across a cell membrane, water must enter the cell through, for example, an aquaporin channel. We investigated sugar transport in OHCs by analyzing the change in cell volume when external D-glucose, normally present in extracellular saline, was replaced isotonically by fructose. Isotonic glucose replacement produced a shortening of the cell (**Fig. 1**). The simultaneous measurement of cell width and length (**Fig. 1b**) indicated that the cell volume increased (**Fig. 1c**). Such volume changes were reversible in all cells tested. Glucose replacement for periods longer than 40 seconds produced a sustained length change with no sign of relaxation. Even after 100 seconds, cells returned to control lengths when glucose was reintroduced. In a population of 5 cells taken from the middle turns of the cochlea (mean cell length 53 μm), length decreased by 2.1 ± 0.4 μm (mean ± s.d.) after 30 seconds of perfusion (**Fig. 1d**).

The specificity of sugar transport was studied by replacing external glucose with other sugars for 30 seconds (**Fig. 1d**). In OHCs with a mean length of 50 μm, little change in cell length was observed when glucose was replaced with sucrose or mannose, although D-galactose produced a decrease in length similar to that found with D-fructose. Six different isoforms (GLUT1–6) of the facilitative hexose transporter are known in mammalian cells. Of these, only GLUT5 preferentially transports fructose. The GLUT2 isoform transports fructose in the absence of glucose, but its action is blocked, as in the isoforms GLUT1 and 3, by cytochalasin B acting on the cytoplasmic surface[18,19]. Cytochalasin B (10 μM) was added to all bath solutions for at least 20

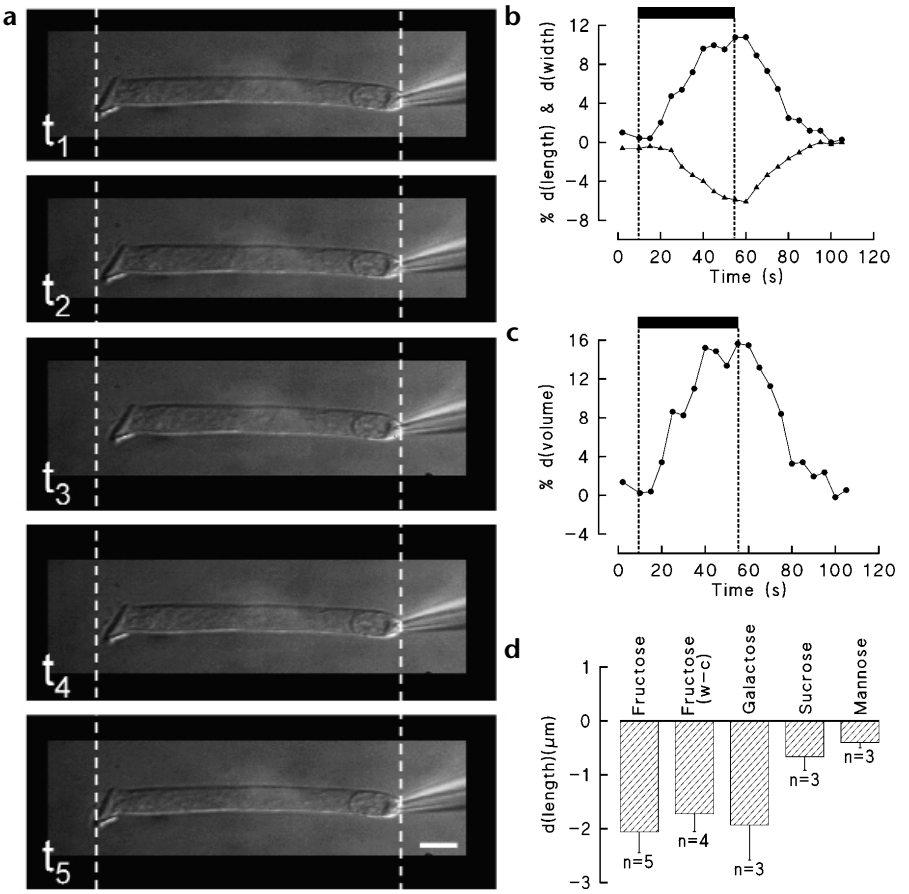

Fig. 1. Outer hair cell volume change induced by replacement of sugars. **(a)** Isotonic replacement of 28 mM glucose with fructose. Images were taken before (t_1 = 0 s), during (t_2 = 20 s, t_3 = 40 s) and after (t_4 = 70 s, t_5 = 105 s) perfusion. The cell was attached to a pipet on its basal pole to avoid drift in position, and the perfusion pipet was positioned 40 μm away. Scale bar, 10 μm. **(b)** Cell length and width change during fructose application (bar). Measurements were made every five sampled images from the cell shown in **(a)**. The short delay observed before any change in cell length was due to the delivery time for replacing sugars outside the cell. **(c)** Volume change computed from **(b)** by assuming a cylindrical cell model. **(d)** Length change after 30-s isotonic replacement of glucose with fructose (cell free) and in whole-cell clamp configuration (fructose wcc; holding potential, −50 mV), galactose (cell free), sucrose (cell free) or mannose (cell free). Error bars show standard deviations.

minutes before sugar exposure, allowing enough time for the drug to permeate the OHC membrane. Under these conditions, there was no significant difference in cell length change produced either by galactose ($n = 3$) or by fructose ($n = 3$) compared with controls without the compound. Because only GLUT2 and GLUT5 have been reported to transport fructose[20], we conclude that GLUT2, if present on the basolateral membrane, cannot be responsible for fructose transport. GLUT5 or a closely related isoform, also insensitive to cytochalasin B, must therefore be responsible for fructose and possibly galactose[21] uptake.

Expression of a sugar transporter in OHCs

To determine whether guinea-pig hair cells expressed GLUT5, we used *in-situ* hybridization on the organ of Corti. Antisense GLUT5 riboprobes labeled the three rows of guinea pig OHCs (**Fig. 2a**). Immunohistochemical evidence from gerbil[17], mouse and human (A.F. unpublished observations) suggests that GLUT5 can be detected along the length of the OHC basolateral membrane. GLUT5 antibodies raised against the *C*-terminal end of the protein labeled guinea-pig OHC, with a circumferential localization below the level of the cuticular plate at the apical portion of the cell (**Fig. 2b**). The labeling was variable, and other antibodies can detect a GLUT5 signal down the entire basolateral membrane (B. A. Schulte, personal communication). GLUT2 antibodies did not demonstrate any significant immunolabeling (data not shown), consistent with the functional studies described above.

Interactions between sugars and the OHC motor activity

These length and volume changes (**Fig. 1**) occur on a time scale of seconds, whereas fast OHC electromotility occurs on a time scale of microseconds. Surprisingly, sugars affected fast electromotility by altering the voltage dependence of charge movement. In such electrophysiological experiments, the presence of a patch pipet in whole-cell recording mode did not affect cell shortening. Isotonic replacement of glucose with fructose produced a cell shortening of 1.7 ± 0.3 μm ($n = 4$) in a patch-recorded cell (**Fig. 1d**), which was not significantly different from unpatched intact cells (*t*-test, $p > 0.05$).

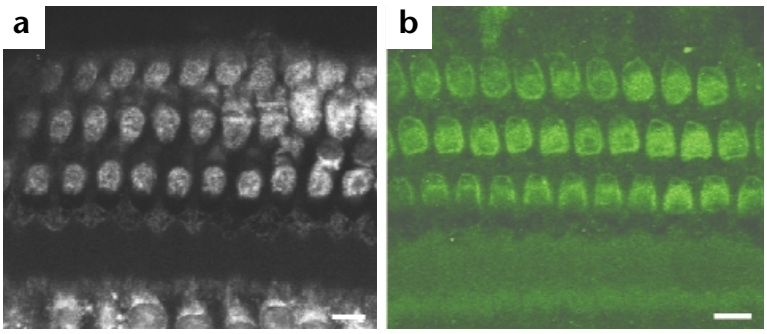

Fig. 2. GLUT5 expression in the organ of Corti. **(a)** Antisense GLUT5 riboprobes labeled the three rows of guinea pig OHCs in whole-mount preparations. **(b)** The three OHC rows were strongly immunoreactive for GLUT5. No signal was observed from the inner hair cells. The mounted preparation, from young adult guinea pigs, was chosen to show antibody binding at the level of the cuticular plate and extending down the basolateral membrane. Scale bars, 10 μm.

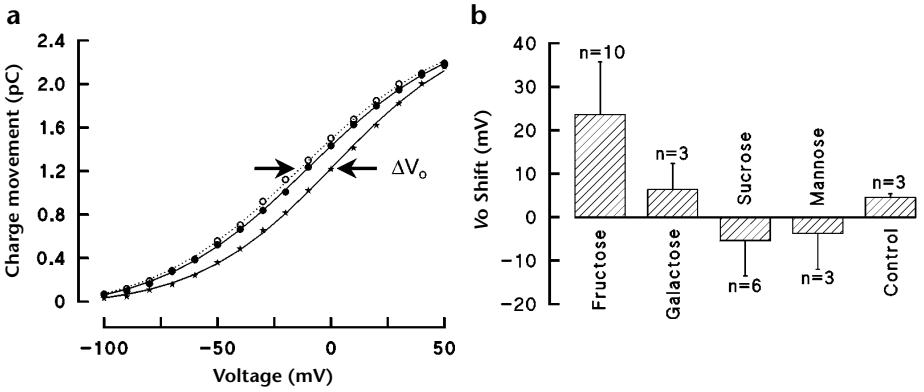

Fig. 3. Sugar transport affects charge movement in OHCs. **(a)** *Q–V* curves in control conditions (28 mM extracellular glucose; ●), 30 s after glucose–fructose replacement (★) and 30 s after return to control (O). Holding potential, –50 mV. Parameters for the *Q–V* curve (see Methods), β = 0.03 mV^{-1}, Q_{max} = 2.56 pC and V_o = –10.0 mV (in glucose), 1.3 mV (in fructose) –13.6 mV (after washout). **(b)** The shift in V_o induced by different sugars. Measurements were made using the same protocol as in **(a)** before and one minute after perfusion and two minutes after washout. Fructose was applied to 10 OHCs held at –50 mV. Initial V_0 value, –42.6 ± 15.3 mV at –50 mV. Galactose, sucrose and mannose were also applied to OHCs held at –50 mV. Initial V_0 values, –42.2 ± 22.8 mV (n = 3) with galactose, –40.7 ± 11.7 mV (n = 6) with sucrose and –35.7 ± 30.9 mV (n = 3) with mannose. The effect of volume increase alone was tested in 3 cells bathed in a saline sucrose solution (325 mosmol per kg; 30 mM sucrose) and perfused for 2 minutes with a hypotonic solution (315 mosmol per kg; 20 mM sucrose). Initial value for V_0, –66.9 ± 12.0 mV (n = 3). Error bars show standard deviations.

The voltage dependence of OHC charge movement was fitted by a Boltzmann function[9,11]. In such *Q–V* curves, V_0 parameterizes the midpoint of the curve and is the voltage at which the charge is equally distributed between inside and outside of the membrane[10,11]. At a holding potential of –50 mV, isotonic replacement of glucose with fructose induced a reversible positive shift (ΔV_0) of the *Q–V* curve (**Fig. 3**). For fructose, ΔV_0 was +23.5 ± 12.1 mV (n = 10). In three additional cells, the shift in V_0 was associated with a comparable shift in the voltage dependence of the length change (data not shown). However, isotonic replacement of glucose with sugars other than fructose did not significantly alter the *Q–V* curve. Sucrose (ΔV_0 = –5.4 ± 8.1 mV, n = 6), galactose (ΔV_0 = 6.4 ± 6.0 mV, n = 3) and mannose (ΔV_0 = –3.7 ± 8.3 mV, n = 3) produced shifts in V_0 not significantly different from 0 mV.

OHC charge movements can also be characterized by changes in membrane capacitance, as the presence of a tethered charge Q moving in the membrane gives rise to an apparent voltage-dependent membrane capacitance, $C_v = dQ/dV$. The maximum of C_v occurs at V_0, and any change in V_0 will produce an apparent change in the cell capacitance when measured at a fixed potential. In particular, at holding potentials more negative than V_0, a positive shift ΔV_0 of the underlying *Q–V* curve will result in a reduction in measured cell capacitance. Such changes were used to follow the effects of sugar replacement.

At a fixed potential, whole-cell capacitance changed following isotonic replacement of glucose with fructose (**Fig. 4**). The capacitance reduction was consistent with a positive shift of V_0. The change occurred with a time constant ($\tau_{1/2}$) of 3.7 seconds, limited by the slow rate of sugar perfusion around the cell. Measured simultaneously, however, the cell length decreased more slowly with $\tau_{1/2}$ of 8.0 seconds. This suggests that cell capacitance and volume changes were significantly decoupled from each other and that mechanical stresses in the cell membrane cannot account for the change in the *Q–V* curve. The faster time constant was not a consequence of the non-linearity of the capacitance voltage curves. When cells were held at potentials between –80 and –40 mV, negative to V_0, they exhibited similar kinetics, with time constants ranging between 2 and 4 seconds.

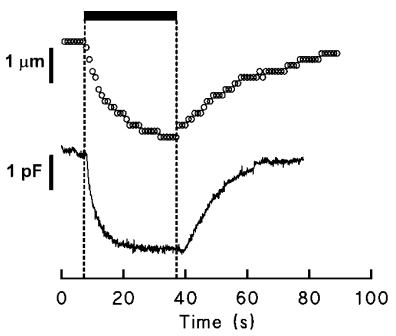

Fig. 4. Time course of extracellular fructose action. Fructose induced a reversible change of cell length (top) and cell capacitance (bottom) with near complete recovery after 60 s. The maximum change in cell length was 2.4 µm. Maximum capacitance decrease, 3.0 pF. Half times for cell length and capacitance decreases were $\tau_{1/2}$ = 8.0 s and 3.7 s, respectively. Capacitance recovered with $\tau_{1/2}$ = 11.3 s and length recovered with $\tau_{1/2}$ = 26.1 s.

Two types of experiment were done to exclude the contribution of membrane stress to ΔV_0, as it is known that stretching the OHC membrane can result in a measurable capacitance decrease[22,23]. First, replacement of external sucrose by hypo-osmotic solution (20 mM sucrose replacing 30 mM sucrose) produced a length change of approximately 2 µm. The computed change in cell volume (11%) was close to that found for fructose replacement, but the associated shift ΔV_0 = +4.6 ± 0.8 mV (n = 3) was much less than that produced by fructose. Removal of all external sucrose (making the bathing solution hypo-osmotic by 30 mosmol per kg) produced a mean shift ΔV_0 of +12.5 mV. In this case, the cell shortened by 6 µm after 60 seconds of perfusion. This indicates that large membrane strains are required for comparable ΔV_0 values. We estimate that at most 20% of the electrical effects found for isotonic glucose–fructose replacement can be accounted for by membrane tension. The same conclusion can be reached from experiments where much larger hypo-osmotic shocks are delivered to the cell[22]. Secondly, to minimize the effects of membrane stretch, we measured cell capacitance in excised membrane patches. Using inside-out patches from the lateral OHC membrane, a capacitance decrease of 8 fF, or approximately 8% of the total nonlinear capacitance was observed when 5 mM fructose solution was applied (**Fig. 5c**). A mean shift ΔV_0 of +12.5 ± 9.3 mV (n = 3) was measured in these conditions.

We investigated the possibility that the influx of water following sugar entry reduced intracellular ionic strength. By altering the surface charge on the inside of the basolateral membrane, this could have modified the measured nonlinear charge movement and consequently the apparent cell capacitance. Capacitance was

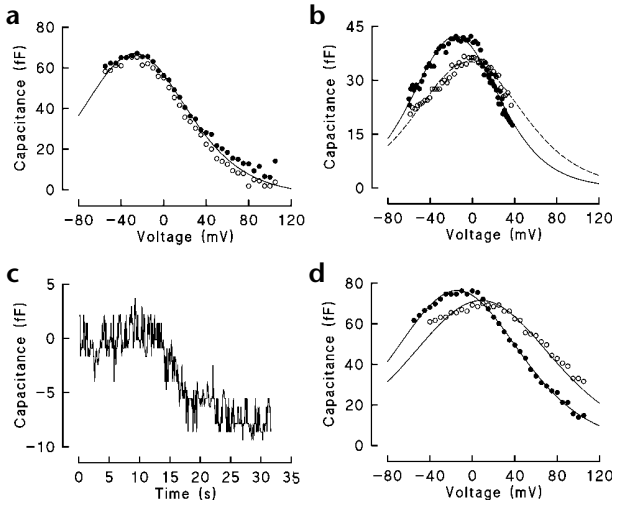

Fig. 5. Effect of fructose on capacitance in basolateral membrane patches. **(a)** Extracellular replacement of 5 mM sucrose with 5 mM fructose in a cell-attached patch before excision. Membrane patch held at 0 mV. Fructose had no significant effect on membrane capacitance. V_0 = –27 mV for both control (●) and perfused (O) conditions after 30 s perfusion. **(b)** Extracellular replacement of 28 mM glucose with 28 mM fructose induced a small depolarizing shift of the curve with V_0 = –15.8 mV in glucose (●) and V_0 = –2.8 mV after 50 s fructose perfusion (O). Membrane patch held at –10 mV. **(c)** Effect of 5 mM fructose, replacing 5 mM sucrose on the intracellular surface of an excised inside-out patch held at 0 mV. **(d)** Voltage-dependent patch capacitance in an excised patch, 5 mM fructose replacing 5 mM sucrose on the intracellular surface. Fructose produced a shift of the *C–V* curve with V_0 at –14.3 mV (control, ●) to +8.4 mV after 30 s perfusion (O). Excised inside-out patch held at 0 mV. Parameters for *C–V* curves (see Methods), in **(a)**, V_0 = –27.0 mV, β = 0.030 mV^{-1}, Q_{max} = 9.3 fC; in **(b)** before perfusion, V_0 = –15.8 mV, β = 0.036 mV^{-1}, Q_{max} = 4.7 fC; in **(b)** during perfusion, V_0 = –2.8 mV, β = 0.030 mV^{-1}, Q_{max} = 4.7 fC; in **(d)** before perfusion, V_0 = –14.3 mV, β = 0.025 mV^{-1}, Q_{max} = 12.3 fC and in **(d)** during perfusion, V_0 = +8.4 mV, β = 0.022 mV^{-1}, Q_{max} = 13 fC. **(a,c,d)** data collected from the same cell.

recorded from the lateral wall in cell-attached configuration. No significant capacitance change (ΔV_0 = +1.6 mV, n = 3) was observed, after 30 seconds, when 5 mM glucose was replaced by 5 mM fructose around the rest of the cell (**Fig. 5a**). This result excludes a change in surface charge as responsible for ΔV_0. It also suggests that intracellular fructose has little effect at this lower concentration. However, it should be noted that a larger shift ΔV_0 of +9.2 ± 4.9 mV (n = 3) was observed after 50 seconds of isotonic replacement of 28 mM glucose with fructose (**Fig. 5b**).

Site of action of sugars

To identify where sugars acted, isotonic fructose was applied from a small-diameter pipet at different restricted sites along the OHC membrane (**Fig. 6a**). The sugar produced a capacitance decrease when applied at apical, middle and basal locations along the cell, indicating that its target lies along the entire basolateral membrane. To ascertain whether this was due to local mechanical stretch of the membrane, control solutions with glucose were also applied to the cell (**Fig. 6b**). No changes in capacitance were then observed.

Discussion

The OHC motor has so far been characterized best by its electrical properties. From measurements of charge movement, it is known that about 7500 single charges move across each square micron of membrane during mechanical activity of the OHCs[24], and this number is approximately the same as particle density in the lateral OHC plasma membrane[25]. The hypothesis that the motor protein is a sugar transporter is supported by the following morphological, physiological and electrophysiological data.

First, a fructose transporter GLUT5 is expressed in guinea-pig OHCs. It is present in the basolateral membrane of gerbil, mouse and guinea pig OHCs. In gerbil OHCs, the system where data are most complete, GLUT5 appears as early as postnatal day 10 (ref. 17). This expression correlates well with the appearance of basolateral membrane particles[26]. In gerbil, auditory function is established by day 12.

Second, the size of motor particle in OHCs[8] is compatible with the reported membrane structure of the fructose transporter GLUT5. Members of the facilitative hexose transporters are integral membrane proteins containing 12 transmembrane α-helices, with molecular weights of 50–55 kDa depending on the isoform[27]. They are found in membranes in both dimeric and tetrameric forms[28,29]. Using 1.40 nm^2 (ref. 30) as the area per helix, the (lower) estimate for the diameter the OHC motor particle (8 nm; ref. 8) would correspond to 4 glucose transporters with a combined molecular weight of 220 kDa. A tetrameric structure has already been proposed as an attractive model for the motor, as it allows rapid reorganization of the subunits to generate an area change[31]. Two major bands obtained by western blotting of extracted membrane proteins from OHCs lie at 55 kDa and 220–240 kDa (ref. 32), and only subcomponents of these bands have been identified with tubulin and spectrin, respectively.

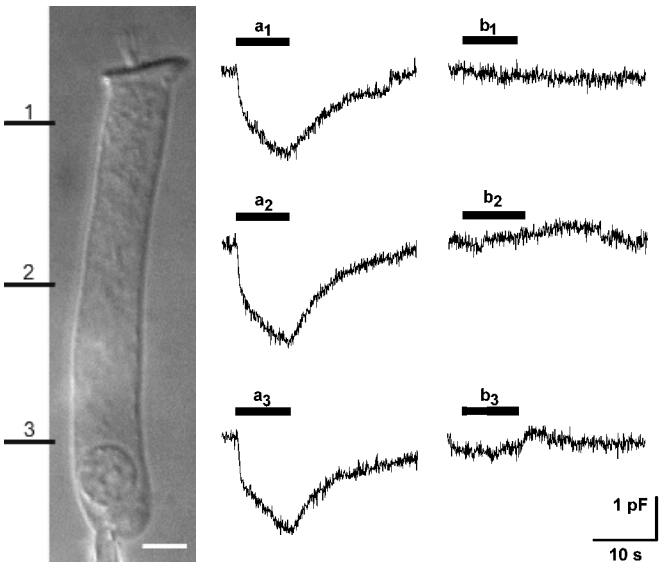

Fig. 6. Localization of the capacitance change produced by fructose. Apical (1), middle (2) and basal (3) sites of application. **(a)** Application of isotonic fructose solution from the puff pipet produced a decrease of membrane capacitance at all three positions. **(b)** No change occurred when control glucose solution was applied. A representative cell is shown patched at its basal pole and the positions of solution application are illustrated. Cell holding potential, –50 mV. Scale bar, 5 μm.

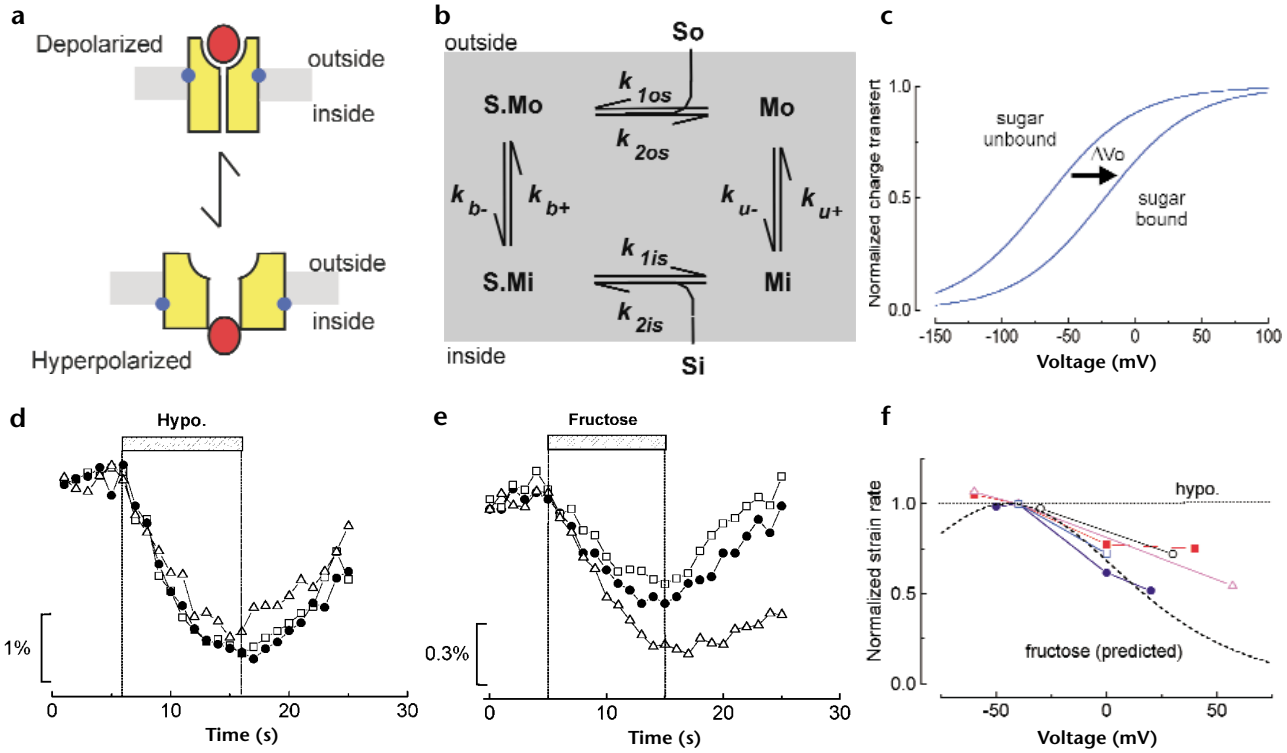

Fig. 7. A kinetic scheme for the outer hair cell motor. **(a)** Schematic model of a sugar (red circle) binding to the two-state, variable-area transporter. The charge on the transporter (blue circle) and conformation change are linked. **(b)** The kinetic scheme is a four-state model for a carrier that transfers sugar (S) from outside to inside of the cell. A single positive charge on the outside is associated with states M_o and $S.M_o$ and on the inside with states M_i and $S.M_i$. The states M_o and M_i represent the transporter in its unloaded configuration. To ensure that the charge movement has relaxation times on the order of 10^{-4} s, the transition rates for the bound or unbound states between the inside and outside states were chosen to be of order 10^5 s^{-1}. To obtain physiological sugar transport rates, rate constants for the binding steps are three orders of magnitude less than the translocation steps. **(c)** Charge translocation curves predicted with and without external sugar $[S]_o$ = 30 mM. Parameters, $k_{1os} = k_{2is}$ = 100 s^{-1} mM^{-1}; $k_{2os} = k_{1isl}$ = 100 s^{-1}; $k_{u-} = 1 \times 10^4 \exp(-\beta V)$ s^{-1}; $k_{u+} = 1.4 \times 10^5 \exp(+\beta V)$ s^{-1}; $k_{b-} = 3\ k_{u-}$ and $k_{b+} = 0.5\ k_{u+}$, β = 0.015 mV^{-1}. The parameters were chosen to set V_0 = –22 mV (–67 mV) in the fully bound (unbound) state of the transporter. The voltage sensitivity β is compatible with published *Q–V* curves[9–11]. **(d)** Cell shortening induced by reducing tonicity of bathing sucrose solution by 10 mosmol per l for 10 s at –70 mV (Δ), 0 mV (●) and +67 mV (□). **(e)** Cell shortening produced by 10 s fructose replacement at –50 mV (Δ), 0 mV (●) and +20 mV (○). Potential commands were applied in a pseudorandom order. The vertical bar in **(d)** and **(e)** is the measured cell strain. **(f)** Collected data for voltage sensitivity of sugar transport. The initial rate of OHC shortening to 10 s exposure to isotonic fructose at different holding potentials. Data has been selected from 5 cells held stably for up to 400 s and normalized to values at –40 mV. The dashed curve predicted for fructose is plotted using the kinetic model parameters in **(c)**. The dashed horizontal line represents the voltage independence of cell shortening induced by hyposmotic solution. Whole-cell recording conditions.

Third, the OHC swelling rate (**Fig. 1**) can be used to estimate the number of transporters in outer hair cells. An OHC 50 µm long has a volume of 3.9 pl and thus, a 15% volume increase in 10 seconds after 30-mM fructose exposure requires a net influx 7×10^9 sugars per cell per second. If we use an estimated turnover rate of 350 per second per GLUT5 monomer, consistent with the transport rates for GLUT isoforms in other tissues[33], each cell must have contained 2×10^7 transporters (or 5×10^6 tetrameric units). Despite the approximate nature of the calculation, this latter number is a lower bound. It is in reasonable agreement with the estimates for the motor particle density[8,11].

Our proposal for the motor depends on combining data from both transport and protein conformation studies. A simple model that brings the observations together is an extension of a four-state model used to describe carrier transport[34] (**Fig. 7**). The additional assumptions are, first, that the transporter has two different area configurations depending on whether its binding site is exposed on the inside or on the outside, second, that equilibrium of the transporter is voltage sensitive and, third, that the equilibrium configuration of the transporter depends on its binding to the sugar. Charged sidegroups of the transporter would be expected to confer voltage sensitivity on the transporter and make the transition rates and equilibrium configurations of the transport dependent on membrane potential. Such mobile charges present in the molecule are those that are detected electrophysiologically as a charge movement, and hence the *Q–V* curve also becomes a measure of the equilibrium configuration of the transporter.

In this model, V_0 of the *Q–V* curve reflects whether the transporter has a sugar molecule bound to it. With the assumptions made about the rate constants in Fig. 7, the high affinity of the transporter for fructose ensures that the transporter is approximately equidistributed between inside and outside states in the presence of fructose, and hence the V_0 has a relative positive value. The low affinity for a sugar such as mannose leaves the transporter in the unbound state, and V_0 consequently moves in

the negative direction. We make no distinction between the affinity of the sites on the inside and outside, but an asymmetry in binding may be responsible for the behavior of individual sugars such as galactose. It should be noted that the explicit movement of sugar does not determine the transition of the charge conformers (which we assume in this model to be fast): the sugar affects only the equilibrium configuration of the transporter.

The interaction of sugar with its binding site at the membrane, and not the translocation, remains the rate-limiting step that determines overall sugar flux in this model. The model predicts, therefore, that fructose transport across the membrane should be affected by membrane potential, V. Solving the kinetic equations of the model, it can be shown that the initial sugar transport rate ($= dS_i/dt$) is proportional to

$$k_{b-}/(k_{b-} + k_{b+}) \cdot k_{u+} / (k_{u-} + k_{u+})$$

where the rates k_i defined in Fig. 7 depend on V.

This prediction was tested by exposing voltage-clamped cells to isotonic fructose solutions and using the initial rate of cell shortening as a measure of sugar transport rate. Over a 140-mV range (–70 mV to +70 mV), cell shortening rates and hence volume changes induced by hypo-osmotic solutions were voltage independent (**Fig. 7d**). However, over the range from –60 to +60 mV, length changes induced by glucose–fructose replacement did depend on membrane potential (**Fig. 7e** and **f**). The initial shortening rate at 0 mV was 70% of the rate at –40 mV. In all cells where sufficiently stable recordings were obtained, larger reductions were measured at more depolarized potentials. In addition, the predicted voltage dependence provides a good fit to the measured cell shortening rates (**Fig. 7f**). These data suggest that in other systems a number of hitherto 'neutral' transporters may show fluxes that are potential dependent.

The proposed identification of the OHC motor with a sugar-transporting protein related to GLUT5 suggests why the protein has proved difficult to identify. The distinguishing feature of the mammalian OHC may not be the expression of a protein specific to the cochlea but the ability to insert a protein found widely in other tissues into its basolateral membrane at high density. The precise structural basis for the conformational change and force generation by the OHC motor remains to be determined.

Methods

Cell preparation. Adult guinea pigs (200–400 g) were killed by rapid cervical dislocation, and both bullae were removed. All animal care facilities and experiments were regulated under UK Home Office guidelines. The organ of Corti was dissected in standard saline containing 145 mM NaCl, 4 mM KCl, 1 mM $CaCl_2$, 1.5 mM $MgCl_2$, 5 mM HEPES and 28 mM D-glucose, pH 7.35, 325 mosmol per kg. The tissue was then bathed in 0.25 mg per ml trypsin (Sigma) for 10 min before gentle mechanical dissociation. The cells were transferred to a 0.5-ml chamber mounted on the stage of an inverted microscope (IM, Zeiss, Germany). The bath solution was continuously perfused at a rate of 100 µl per min. Cells were used within three hours of dissection. Experiments were done at room temperature (20–25°C).

Recording. Conventional patch-clamp techniques were used[35]. Patch pipets were pulled on a two-stage vertical puller using 1.2-mm outer diameter thin-walled borosilicate glass capillaries (GC120TF, Clark Electromedical Instruments, UK) and had resistances of 2–4 MΩ measured in the bath. No active series resistance compensation was used, but pipets were coated with ski wax (Toko, Switzerland) to minimize stray capacitance[36]. For whole-cell voltage-clamp experiments, pipets were filled with intracellular solution designed to reduce ionic currents containing 114 mM NaCl, 30 mM TEA, 2.5 mM $MgCl_2$, 6 mM EGTA and 10 mM HEPES, pH 7.30, with D-glucose added to 325 mosmol per kg. The removal of macroscopic ionic currents allowed good isolation of the charge displacement currents[14]. For membrane patch experiments, the pipet solution contained 138 mM NaCl, 4 mM KCl, 7 mM $BaCl_2$, 1 mM $CaCl_2$, 1.5 mM $MgCl_2$ and 5 mM HEPES, with D-glucose added to 300 mosmols per kg. Barium was used to block any residual lateral K^+ channels. Gigaseal recordings were made on the lateral membrane of OHCs.

Transient currents obtained on stepping the potential for 5 ms in 10-mV increments from –120 mV were used to determine the motor charge movement[23,37]. The charge–voltage (Q–V) curve was fitted with a Boltzmann function:

$$Q(V) = \frac{Q_{max}}{1 + \exp[-\beta(V - V_o)]} \quad (1)$$

where V_0 is the symmetrical midpoint of the curve. Nonlinear capacitance was measured by AC analysis using a lock-in amplifier technique[38,39] implemented in software[11] or, for patches, with an analog amplifier (SR530, Stanford Research, USA). A 10 mV, 1 kHz sinusoidal command was applied to the cell during a ramped potential, and current amplitude and phase were computed[14]. The nonlinear capacitance–voltage (C–V) curve was fitted by

$$C_V = \frac{dQ}{dV} = \frac{\beta Q_{max} \exp[-\beta(V - V_o)]}{\{1 + \exp[-\beta(V - V_o)]\}^2} \quad (2)$$

Capacitance records were calibrated using a 100 fF dither signal implemented in the patch amplifier circuit.

For experiments involving isotonic replacement of D-glucose, solutions were applied through a perfusion pipet with a tip 2 µm in diameter positioned 30–40 µm away. Pressures of 8–12 cm-H_2O were used to eject solutions. To verify that the whole cell and not only a small area was perfused, control experiments included a fluorescent dye in the pipet solution. When localized superfusion was done, smaller pipets were used (tip diameter under 1 µm), which were positioned 10 µm away from the cell. It was found that no more than 30% of the cell received solution.

Imaging. Cell images were captured at either 1 or 2 Hz by a high-resolution video camera using Axon Imaging Workbench software (Axon Instruments, USA). The captured pixel width was 114 nm. Image processing was enhanced using MATLAB 5.3 (Mathworks, USA). Cell length and width changes were estimated by following the position of the centroid of boundary pixels located at the cuticular plate, the base of the cell and at the lateral surfaces. We estimate that the errors in cell length and width measurements did not exceed 15%.

***In-situ* hybridization.** Cochlear tissue, fixed in 4% paraformaldehyde, was dehydrated in ethanol and incubated with FITC-labeled riboprobes. Sense and antisense probes were generated by T3 and T7 RNA polymerase using as template a pCR-Script plasmid (Stratagene, USA) containing a mouse GLUT5 insert amplified by RT-PCR using sequence information from EST AA472264, position 16 to 148. Hybridization was done in 4× SSC, 2 mg per ml BSA and 20% dextran sulphate for 16 h at 37°C. Samples were washed with 50% formamide and 2× SSC, 5 × 3 min and then with 2× SSC alone, 5 × 3 min. Sections were then mounted on polylysine coated slides in Slowfade (Molecular Probes, USA) and viewed by confocal microscopy.

Immunohistochemistry. Immunostaining was done on whole-mount preparations and frozen sections of cochlear tissues fixed in 4% paraformaldehyde. Whole-mount preparations were permeabilized with 0.3% Triton X-100 for 15 min. Samples were pre-blocked in 5% horse serum in PBS before incubation with primary antibody overnight at 4°C. Anti-GLUT5 and anti-GLUT2 antibodies (Chemicon International Ltd, UK) raised in rabbits were diluted between 1:100 and 1:1000. The samples were incubated in biotinylated goat anti-rabbit secondary antibody (1:150), then in FITC-conjugated streptavidin (1:150). Samples were mounted on slides with a glycerol buffer containing anti-bleaching agent. For negative controls, either the primary antibody was omitted or samples were exposed to non-immune rabbit serum. Positive controls for GLUT5 were obtained from guinea pig testis and intestine, and for GLUT2 from liver.

Acknowledgements

This work was supported by the Wellcome Trust. We thank Matthew Holley, Peter Mobbs and Luca Turin for comments on an earlier version of the manuscript. S.O.C. is supported by a George John Livanos Charitable Trust Fellowship.

Received 21 May; accepted 22 June 1999

1. Davis, H. An active process in cochlear mechanics. *Hearing Res.* **9**, 79–90 (1983).
2. Russell, I. J., Cody, A. R. & Richardson, G. P. in *Cellular Mechanisms in Hearing* (eds. Flock, A. & Wersäll, J.) 199–216 (Elsevier, Amsterdam, 1986).
3. Brownell, W. E., Bader, C. R., Bertrand, D. & De Ribaupierre, Y. Evoked mechanical responses of isolated cochlear hair cells. *Science* **227**, 194–196 (1985).
4. Ashmore, J. F. A fast motile reponse in guinea-pig outer hair cells: the cellular basis of the cochlear amplifier. *J. Physiol. (Lond.)* **388**, 323–347 (1987).
5. Kachar, B., Brownell, W. E., Altschuler, R. & Fex, J. Electrokinetic shape changes of cochlear outer hair cells. *Nature* **322**, 365–368 (1986).
6. Holley, M. C. & Ashmore, J. F. On the mechanism of a high frequency force generator in outer hair cells isolated from the guinea pig cochlea. *Proc. R. Soc. Lond. B Biol. Sci.* **232**, 413–429 (1988).
7. Iwasa, K. H., Li, M. & Jia, M. Can membrane proteins drive a cell? *Biophys. J.* **68**, 214s (1995).
8. Kalinec, E., Holley, M. C., Iwasa, K. H., Lim, D. J. & Kachar, B. A membrane-based force generation mechanism in auditory sensory cells. *Proc. Natl. Acad. Sci. USA* **89**, 8671–8675 (1992).
9. Ashmore, J. F. Forward and reverse transduction in the mammalian cochlea. *Neurosci. Res. (Suppl.)* **12**, 39–50 (1990).
10. Santos-Sacchi, J. Reversible inhibition of voltage-dependent outer hair cell motility and capacitance. *J. Neurosci.* **11**, 3096–3110 (1991).
11. Gale, J. E. & Ashmore, J. F. The outer hair cell motor in membrane patches. *Pflugers Arch.* **434**, 267–271 (1997).
12. Knipper, M. *et al.* Immunological identification of candidate proteins involved in regulating active shape changes of outer hair cells. *Hearing Res.* **86**, 100–110 (1995).
13. Kalinec, F., Kalinec, G., Negrini, C. & Kachar, B. Immunolocalization of anion exchanger 2α in auditory sensory hair cells. *Hearing Res.* **110**, 141–146 (1997).
14. Gale, J. E. & Ashmore, J. F. An intrinsic frequency limit to the cochlear amplifier. *Nature* **389**, 63–66 (1997).
15. Huang, G. & Santos-Sacchi, J. Motility voltage sensor of the outer hair cell resides within the lateral plasma membrane. *Proc. Natl. Acad. Sci. USA* **91**, 12268–12272 (1994).
16. Dallos, P. & Evans, B. N. High-frequency motility of outer hair cells and the cochlear amplifier. *Science* **267**, 2006–2009 (1995).
17. Nakazawa, K., Spicer, S. S. & Schulte, B. A. Postnatal expression of the facilitated glucose transporter, GLUT 5, in gerbil outer hair cells. *Hearing Res.* **82**, 93–99 (1995).
18. Gould, G. W., Thomas, H. M., Jess, T. J. & Bell, G. I. Expression of human glucose transporters in Xenopus oocytes: kinetic characterization and substrate specificities of the erythrocyte, liver, and brain isoforms. *Biochemistry* **30**, 5139–5145 (1991).
19. Colville, C.A., Seatter, M. J. & Gould, G. W. Analysis of the structural requirements of sugar binding to the liver, brain and insulin-responsive glucose transporters expressed in oocytes. *Biochem. J.* **294**, 753–760 (1993).
20. Gould, G. W. & Holman, D. The glucose transporter family: structure, function and tissue-specific expression. *Biochem. J.* **295**, 329–341 (1993).
21. Miyamoto, K. *et al.* Characterization of the rabbit intestinal fructose transporter (GLUT5). *Biochem. J.* **303**, 877–883 (1994).
22. Iwasa, K. H. Effect of stress on the membrane capacitance of the auditory outer hair cell. *Biophys. J.* **65**, 492–498 (1993).
23. Gale, J. E. & Ashmore, J. F. Charge displacement induced by rapid stretch in the basolateral membrane of guinea-pig outer hair cell. *Proc. R. Soc. Lond. B Biol. Sci.* **255**, 243–249 (1994).
24. Huang, G. & Santos-Sacchi, J. Mapping the distribution of the outer hair cell motility voltage sensor by electrical amputation. *Biophys. J.* **65**, 2228–2236 (1993).
25. Forge, A. Structural features of the lateral walls in mammalian cochlear outer hair cells. *Cell Tissue Res.* **265**, 473–483 (1991).
26. Souter, M., Nevill, G. & Forge, A. Postnatal development of membrane specialisations of gerbil outer cells. *Hearing Res.* **91**, 43–62 (1995).
27. Gould, G. W. & Bell, G. I. Facilitative glucose transporters: an expanding family. *Trends Biochem. Sci.* **15**, 18–23 (1990).
28. Pessino, A. *et al.* Evidence that functional erythrocyte-type glucose transporters are oligomers. *J. Biol. Chem.* **266**, 20213–20217 (1991).
29. Zottola, R. J. *et al.* Glucose transporter function is controlled by transporter oligomeric structure. A single, intramolecular disulfide promotes GLUT1 tetramerization. *Biochemistry* **34**, 9734–9747 (1995).
30. Eskandari, S. *et al.* Structural analysis of cloned plasma membrane proteins by freeze-fracture electron microscopy. *Proc. Natl. Acad. Sci. USA* **95**, 11235–11240 (1998).
31. Iwasa, K. H. A membrane motor model for the fast motility of the outer hair cell. *J. Acoust. Soc. Am.* **96**, 2216–2224 (1994).
32. Holley, M. C. A simple in vitro method for raising monoclonal antibodies to cochlear proteins. *Tissue Cell* **24**, 613–624 (1992).
33. Carruthers, A. Sugar transport in animal cells: the passive hexose transfer system. *Prog. Biophys. Mol. Biol.* **43**, 33–69 (1984).
34. Weiss, T. F. *Cellular Biophysics: Transport:* Vol. 1 360–396 (MIT Press, Cambridge, 1996).
35. Hamill, O. P., Marty, A., Neher, E., Sakmann, B. & Sigworth, F. J. Improved patch clamp technique for high resolution current recording from cells and cell free membrane patches. *Pflugers Arch.* **391**, 85–100 (1981).
36. Fuchs, P. A. & Evans, M. G. Potassium currents in hair cells isolated from the cochlea of the chick. *J. Physiol. (Lond.)* **429**, 529–551 (1990).
37. Armstrong, C. M. & Bezanilla, F. Charge movement associated with the opening and closing of the activation gates of the Na channels. *J. Gen. Physiol.* **63**, 533–552 (1974).
38. Neher, E. & Marty, A. Discrete changes of cell membrane capacitance observed under conditions of enhanced secretion in bovine adrenal chromaffin cells. *Proc. Natl. Acad. Sci. USA* **79**, 6712–6716 (1982).
39. Joshi, C. & Fernandez, J. M. Capacitance measurements: An analysis of the phase detector technique used to study exocytosis and endocytosis. *Biophys. J.* **53**, 885–892 (1988).